Scaling analysis of 2D fractal cellular structures

2001 J. Phys. A: Math. Gen. 34 25

(http://iopscience.iop.org/0305-4470/34/1/302)

INSTITUTE OF PHYSICS PUBLISHING JOURNAL OF PHYSICS A: MATHEMATICAL AND GENERAL

J. Phys. A: Math. Gen. **34** (2001) 25–36 www.iop.org/Journals/ja PII: S0305-4470(01)12077-9

Scaling analysis of 2D fractal cellular structures

Gudrun Schliecker

Max-Planck-Institut für Physik Komplexer Systeme, Nöthnitzer Str. 38, D-01187 Dresden, Germany

Received 23 February 2000, in final form 20 October 2000

Abstract

The correlations between topological and metric properties of fractal tessellations are analysed. To this end, Sierpinski cellular structures are constructed for different geometries related to Sierpinski gaskets and to the Apollonian packing of discs. For these geometries, the properties of the distribution of the cells' areas and topologies can be derived analytically. In all cases, an algebraic increase of the cell's average area with its number of neighbours is obtained. This property, unknown from natural cellular structures, confirms previous observations in numerical studies of Voronoi tessellations generated by fractal point sets. In addition, a simple rigorous scaling resp. multiscaling properties relating the shapes and the sizes of the cells are found.

PACS numbers: 8717A, 0240S, 6143H

1. Introduction

During the past two decades, the geometric characterization of two-dimensional cellular structures has attracted increasing interest among physicists [1]. Cellular structures can be considered as subdivisions of the plane by polygonal cells with varying numbers of sides (*topologies*). Three cell boundaries always join at the vertices fixing the mean cell's topology to six. The investigation of various *natural* planar tessellations reveals surprising structural similarities among the different systems. These similarities are manifested in different empirical laws for the distributions of the cells' topologies and areas and their correlations [2–5].

Recent experimental and theoretical studies show how these laws are modified in *binary* cellular structures composed of two kinds of cells with different mean areas [6,7] and in *fractal* tessellations with scale invariance [8, 9]. These findings suggest the importance of a unique typical length scale for the structural similarities among most natural planar tessellations. However, up to now only a few of the 'exceptions from the rule' have been investigated in detail. In particular, there are no rigorous results concerning the interplay between metric and topological properties of binary and fractal tessellations.

Only recently, the correlations between the cell's areas and topologies in fractal cellular structures have been studied numerically [9]. This analysis focused on Voronoi tessellations of scale-invariant particle distributions generated by an almost critical directed-percolation

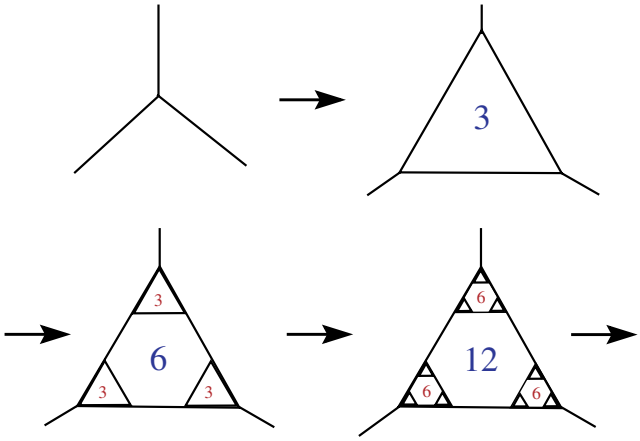

Figure 1. Construction of the Sierpinski cellular structure: the first three iterations.

process in 2 + 1 dimensions. Measuring the relative frequency $P(k, A)$ of k-sided cells with area A, it was observed that curves for different A collapse if they are rescaled appropriately. Therefore, in the scaling regime the scaling relation

$$P(k, A) \sim A^{-\gamma_1} \Phi(kA^{-\gamma_2}) \tag{1}$$

was proposed. Relation (1) leads to an unusual algebraic increase of the mean cell's area with its topology:

$$\langle A \rangle_k \sim k^{1/\gamma_2}. \tag{2}$$

In directed percolation, one has $\gamma_2 = 0.13(3)$, and thus a much faster increase in k than predicted by Lewis's law ($\gamma_2 = 1$) [2]. In [9], the scaling relation (1) has been verified numerically by data collapse. However, each decade of the scaling regime of k requires about five decades of scaling range in A, which is a strong limitation for a numerical verification of relations (1) and (2).

We now address the question whether the relations (1) and (2) can be regarded as a general property of fractal cellular structures. For this purpose, the correlations between topological and metric properties of iteratively constructed fractal tessellations are studied. We focus on Sierpinski cellular structures first constructed in [8], for which the relation between size and shape of the cells has not yet been investigated.

2. Sierpinski gaskets: topology

Natural two-dimensional cellular structures, and those generated by the Voronoi or Laguerre construction, have in common that three edges meet at each vertex [1]. The Sierpinski cellular structures are generated by successive replacements of these trivalent vertices by triangles [8]. In the resulting mosaics, each vertex is replaced by a Sierpinski cellular structure.

In one iteration step, at each vertex a triangle is inserted. The iterations are repeated successively. The first three iterations are represented in figure 1. In the mth step, at each vertex 3^{m-1} new cells are inserted. After M iterations, all cells belonging to a certain generation $m = 1, \ldots, M$ have the same topology

$$k = 3 \cdot 2^{M-m}. \tag{3}$$

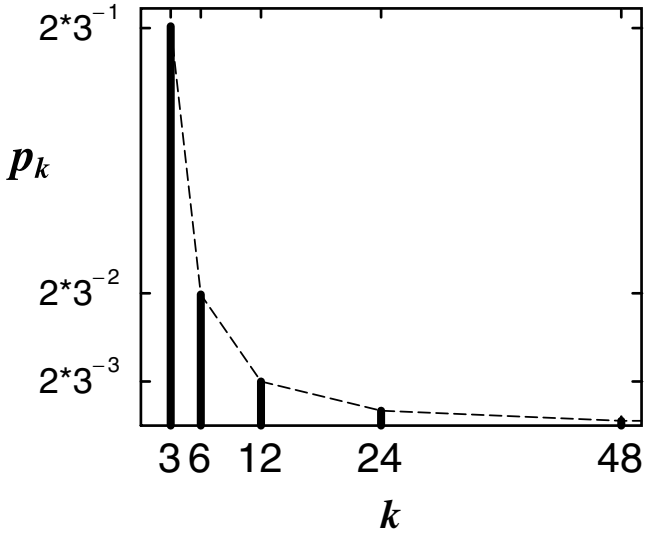

Figure 2. Cell shape distribution p_k for Sierpinski cellular structures.

The topological properties of Sierpinski cellular structures are known [8], in particular the cell shape distribution p_k, defined as the probability for an arbitrarily chosen inserted cell having k sides. Simple calculations yield

$$p_k = \chi(k)\frac{2}{3}\left(\frac{k}{3}\right)^{-\frac{\ln 3}{\ln 2}} \tag{4}$$

where the allowed edge numbers k are selected by the characteristic function $\chi(k) = \sum_{m=1}^{M} \delta_{k,3\cdot 2^{M-m}}$. The cell shape distribution (4) is represented in figure 2. It shows an unusual algebraic decrease.

So far, only the graph of Sierpinski cellular structures has been defined. In order to analyse the interplay between the areas and shapes of the cells in these structures, an appropriate area has to be assigned to each cell. In the following, the metric properties for three typical choices will be analysed.

3. Sierpinski gaskets: metric properties

3.1. Simply scaled cell areas

The first, simplest case is based on the usual construction of the Sierpinski gasket with total area A_Δ, defined as the area of the first inserted triangle (cf figure 1). We now assume that each inserted triangle covers the portion α of one cell of the preceding generation. After M iterations, all cells which belong to a certain generation $m = 1, \ldots, M$ have the same area

$$A(m) = (1 - 3\alpha(1 - \delta_{m,M}))\alpha^{m-1}A_\Delta. \tag{5}$$

Equations (3) and (5) yield a unique relationship between the area of one cell and its topology k:

$$A_k = A_6\left(\frac{k}{6}\right)^{-\frac{\ln\alpha}{\ln 2}} \qquad k = 6, 12, \ldots \tag{6}$$

where $A_6 = (1 - 3\alpha)\alpha^{M-2}A_\Delta$. Only the triangles, for which $m = M$, form an exception with $A_3 = \alpha^{M-1}A_\Delta$. The algebraic variation of A_k in expression (6) results of the exponential decrease in m of both the cells' numbers of edges (3) and their areas (5). Since $0 \leqslant \alpha \leqslant 1/4$, the exponent in equation (6) is always larger than 2, and has no upper limit for infinitesimally small values of α: $-\ln\alpha/\ln 2 \in (2, \infty)$. Consequently, equation (6) agrees with the numerical results in [9], suggesting a fast algebraic increase of $\langle A\rangle_k$ in fractal tessellations.

The scaling relation (1) can also be easily tested for this simple geometry. The relative frequency $P(k, A)$ of k-sided cells with area A reads

$$P(k, A) = p_k\delta(A - A_k). \tag{7}$$

Making use of the results (4) and (6), $P(k, A)$ can be written as

$$P(k, A) = \chi(k)A^{-\gamma_1}\Phi(A^{-\gamma_2}k) \qquad (k \neq 3) \tag{8}$$

where $\Phi(z) = (4/3)A_6^{-\gamma_2+\gamma_1-1}\delta(z - 6 \cdot A_6^{-\gamma_2})$. The exponents are given by $\gamma_1 = 1 - \frac{\ln 3}{\ln\alpha}$, and $\gamma_2 = -\frac{\ln 2}{\ln\alpha}$. Apart from the characteristic function $\chi(k)$, which selects the allowed edge numbers, this equation reproduces the scaling relation (1) proposed in [9].

An equivalent, sometimes more convenient check of the scaling behaviour (1) is based on the q-weighted average area of a k-sided cell:

$$\langle A^q\rangle_k := \frac{\int_0^\infty A^q P(k, A)\,\mathrm{d}A}{\int_0^\infty P(k, A)\,\mathrm{d}A}. \tag{9}$$

In the case that equation (1) holds, one obtains

$$\langle A^q\rangle_k \sim \langle A^q\rangle_6 \left(\frac{k}{6}\right)^{q/\gamma_2}. \tag{10}$$

Thus, a power law in k, where the exponent varies linearly in q, is a characteristic feature of a distribution, for which the scaling relation (1) holds.

3.2. Multiply scaled cell areas

The cells' sizes can be ascribed in a more general way choosing different scaling factors ($\{\alpha_1, \alpha_2, \alpha_3\}, \alpha_i \in (0, 1/4)$) for the areas of the cells inserted at the three vertices of one triangle. Though the cells of one generation still have the same topology, now their areas differ. For the cells of the mth generation ($m = 1, 2, \ldots, M - 1$) they are given by

$$A_{i_1,i_2,\ldots,i_{m-1}}(m) = \alpha_{i_1}\alpha_{i_2}\ldots\alpha_{i_{m-1}}A(1) \qquad \text{with} \quad i_1, i_2, \ldots, i_{m-1} = 1, 2, 3 \tag{11}$$

where $A(1) = (1 - \alpha_1 - \alpha_2 - \alpha_3)A_\Delta$. The relative frequency of k-sided cells ($k \neq 3$) with area A reads

$$P(k, A) = \frac{1}{N}\sum_{m=1}^{M}\delta_{k,3\cdot 2^{M-m}}\sum_{i_1,i_2,\ldots,i_{m-1}=1}^{3}\delta(A - A_{i_1,i_2,\ldots,i_{m-1}}(m)) \tag{12}$$

where N is the total number of inserted cells. From equation (12), the q-weighted average area (9) can be derived easily:

$$\begin{aligned}\langle A^q\rangle_k &= \sum_{m=2}^{M}\delta_{k,3\cdot 2^{M-m}}3^{-m+1}\sum_{i_1,i_2,\ldots,i_{m-1}=1}^{3}[\alpha_{i_1}\alpha_{i_2}\ldots\alpha_{i_{m-1}}A(1)]^q \\ &= \sum_{m=2}^{M}\delta_{k,3\cdot 2^{M-m}}A^q(1)\left[\frac{\alpha_1^q + \alpha_2^q + \alpha_3^q}{3}\right]^{m-1}.\end{aligned}$$

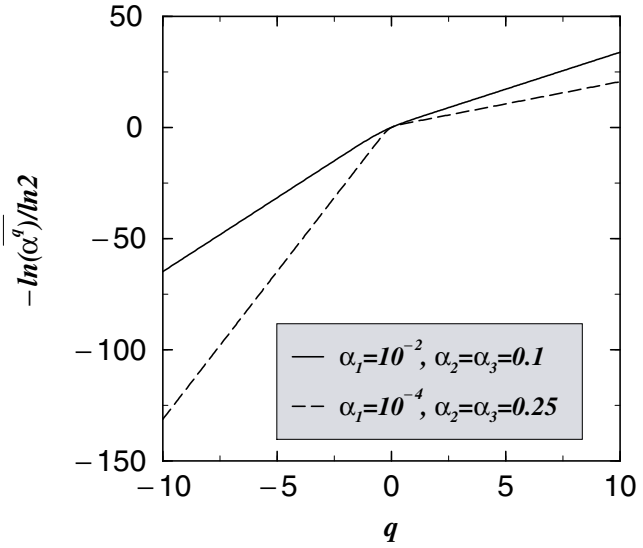

Figure 3. Overall behaviour of the multiscaling exponent in equation (13).

Introducing the notation $\overline{\alpha^q} := (\alpha_1^q + \alpha_2^q + \alpha_3^q)/3$, the final result reads

$$\langle A^q \rangle_k = \langle A^q \rangle_6 \left(\frac{k}{6}\right)^{-\ln \overline{\alpha^q}/\ln 2} \qquad k = 6, 12, \ldots. \tag{13}$$

Again, we obtain an algebraic increase in k. In particular, for $q = 1$ the proposed generalization of Lewis's law for fractal tessellations (2) holds with $\gamma_2 = -\ln 2/\ln \alpha$. For arbitrary values of q, however, the exponents do not vary linearly in q, reflecting that the scaling relation (1) does not hold for different weights $\alpha_1, \alpha_2, \alpha_3$ (see expression (10)). Linearity in q is approached only asymptotically, with a slope determined by the largest scaling factor for $q \to \infty$ and by the smallest scaling factor for $q \to -\infty$. The overall behaviour of the exponent in equation (13) is illustrated in figure 3 for two typical choices of the scaling factors. Its nonlinear variation reflects the multiscaling behaviour of the system. In fact, with different values α_i, this system represents a three-value Cantor set. A multiscaling analysis following the lines introduced in [10] can be performed.

4. Apollonian packing

A Sierpinski cellular structure with a more complex geometry results from the Laguerre tessellation of the Apollonian packing of discs. The construction of the Apollonian packing is defined as follows: the starting point is a curvilinear triangle formed by three mutually touching discs of arbitrary radii. Inside this triangle a new circle touching the three discs is inscribed. This will be later referred to as the seed of the packing. In the next step, new circles are inscribed in the resulting three empty curvilinear triangles. This procedure is repeated iteratively. In each iteration step, a new generation of circles is inscribed. Each circle of the resulting structure is touched by three circles of the next generation, its *daughters*.

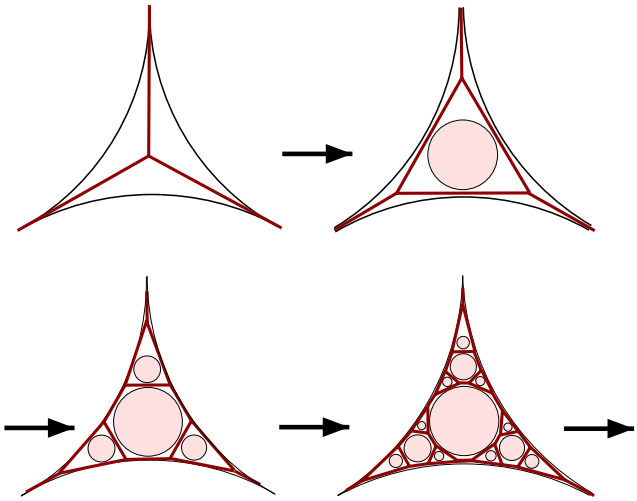

Figure 4. Laguerre tessellations of the Apollonian packing for the first three iterations.

4.1. Laguerre tessellation

A space-filling cellular structure can be associated with this packing, assigning a polygonal cell to each disc. The first attempt might be a Voronoi tessellation [11] generated by the centres of the discs. The Voronoi cell of a disc is defined as the set of points which are closer to its centre than to any other centre. The cell boundaries are composed of straight lines, perpendicular to the connecting line between the centres of two neighbouring discs. Unfortunately, the Voronoi cells may not cover their generating discs completely: whenever two neighbouring discs with different radii touch, the larger disc is cut by its cell boundary. This disadvantage can be circumvented by making use of a different distance definition. In particular, the Laguerre construction [12] has been applied successfully to assemblies of hard discs with different sizes [6]. In the Laguerre tessellation, the distance to a circle is defined as the length of the tangent to the circle. The Laguerre cells are polygons containing their generating disc completely. A sketch of the Laguerre tessellations generated by the Apollonian packing for a few iteration steps is shown in figure 4. From the topological point of view, the insertion of a new circle corresponds to the insertion of a triangle at a vertex, where three cell boundaries meet. Thus, the topological structure is identical with the Sierpinski cellular structure.

The metric properties, however, differ from those obtained in the preceding section. Here we are interested in the area distributions for different generations. For a finite number of iterations, the cell areas would be hard to calculate. But they approach the areas of the generating discs with increasing number of iterations M, since for $M \to \infty$ the Apollonian packing covers the whole area [13].

4.2. Basic metric properties

Our analytical and numerical considerations are based on the well known properties of the Apollonian packing. In figure 5 three mutually touching discs, A, B and C, form a curvilinear triangle with inscribed circle D. The curvatures s_α (α = A, B, C, D) are related by the *Soddy formula* [14, 15]:

$$2(s_A^2 + s_B^2 + s_C^2 + s_D^2) = (s_A + s_B + s_C + s_D)^2. \tag{14}$$

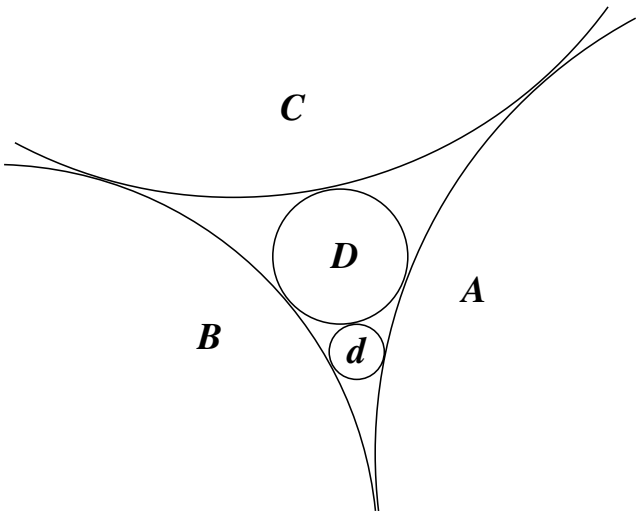

Figure 5. Configuration of the circles A, B, C, D and d in equations (14) and (15).

This equation can be treated as quadratic in s_C with fixed s_A, s_B and s_D. Formally, two solutions are found. One solution just gives s_C, the other solution, s_d, corresponds to the curvature of a circle d which is inscribed in the triangle formed by the circles A, B and D (see figure 5). In this way, a linear identity between the curvatures of the five circles involved can be derived:

$$s_d + s_C = 2(s_A + s_B + s_D). \tag{15}$$

Based on this linear relationship, a *matrix formalism* has been developed for the iterative numerical calculation of the curvatures of the discs [13, 16, 17]. In this formalism, four-vectors, each containing the curvatures of one disc and its circumscribing circles, are calculated iteratively. Since in this representation the generations of the discs cannot be assigned easily, a different matrix representation will be derived here.

In equation (15), d is one of the three *daughters* of D, i.e. a circle of the following generation touching D. A four-vector $\boldsymbol{s}_D = (s_{d_1}, s_{d_2}, s_{d_3}, s_D)^T$ is assigned to D. Its components are the curvatures of D and of its three daughters d_1, d_2 and d_3. Rewriting equation (15) for all daughters of D, the curvatures s_A, s_B and s_C can be expressed as linear combinations of s_{d_1}, s_{d_2}, s_{d_3} and s_D. Applying again identity (15) to the daughters of d_1, d_2 and d_3, linear mappings of $\boldsymbol{s}_D$ on the vectors $\boldsymbol{s}_{d_i}$ can be derived:

$$\boldsymbol{s}_{d_i} = \mathcal{M}_i \boldsymbol{s}_D \qquad i = 1, 2, 3 \tag{16}$$

where $\mathcal{M}_i = \mathcal{M}\mathcal{P}^{i-1}$, and

$$\mathcal{M} = \tfrac{1}{9}\begin{pmatrix} 20 & 5 & -4 & 12 \\ 26 & 2 & 2 & -33 \\ 20 & -4 & 5 & 12 \\ 9 & 0 & 0 & 0 \end{pmatrix} \qquad \mathcal{P} = \begin{pmatrix} 0 & 0 & 1 & 0 \\ 1 & 0 & 0 & 0 \\ 0 & 1 & 0 & 0 \\ 0 & 0 & 0 & 1 \end{pmatrix}. \tag{17}$$

The circle D may be considered as the seed of an Apollonian packing inside the triangle (A, B, C). Thus, iterative application of equation (16) allows one to express the curvature of any disc of an Apollonian packing as a linear combination of the curvatures of the discs of the first two generations contained in $\boldsymbol{s}_D$. The mth generation in an Apollonian packing is the set of discs which originate from its seed after $m - 1$ iterations.

4.3. Moments

We now focus on the properties of the q-weighted sum of curvatures in one generation, or *moment*, defined as

$$\langle S^q\rangle_m(\boldsymbol{s}_{\mathcal{O}}) := 3^{1-m}\sum_{m\text{th gen.}}(s_{\mathrm{d}})^q. \tag{18}$$

The summation runs over all discs d of the mth generation originated from the seed $\mathcal{O}$. The sum over all generations, $\sum_m 3^{m-1}\langle S^q\rangle_m$, the *Melzak function*, is known to diverge for $M\to\infty$ if $q \geqslant -d_{\mathrm{F}}$ [13, 18]. Here, $d_{\mathrm{F}} \simeq 1.306$ is the fractal dimension of the Apollonian packing.

The *average curvature of one generation* ($q = 1$ in expression (18)) can be derived analytically. From equations (16) and (17), a simple recursion relation is obtained:

$$3\langle S\rangle_{l=3}(\boldsymbol{s}_{\mathrm{D}}) - 8\langle S\rangle_{l=2}(\boldsymbol{s}_{\mathrm{D}}) + \langle S\rangle_{l=1}(\boldsymbol{s}_{\mathrm{D}}) = 0. \tag{19}$$

This relation holds for any four-vector $\boldsymbol{s}_{\mathrm{D}}$ in an Apollonian packing. Thus, summation of equation (19) over all discs of the mth generation yields $3\langle S\rangle_{m+2} - 8\langle S\rangle_{m+1} + \langle S\rangle_m = 0$. Here the shorthand notation $\langle S\rangle_m := \langle S\rangle_m(\boldsymbol{s}_{\mathcal{O}})$ omitting the seed vector $\boldsymbol{s}_{\mathcal{O}}$ has been introduced. Thus, the average curvature is given by

$$\langle S\rangle_m = c_+\left(\frac{4+\sqrt{13}}{3}\right)^m + c_-\left(\frac{4-\sqrt{13}}{3}\right)^m.$$

The coefficients $c_\pm$ depend on the curvatures of the circles in the first two generations contained in $\boldsymbol{s}_{\mathcal{O}}$. For large m, the contribution of the larger growth coefficient $\beta(q=1) = (4+\sqrt{13})/3$ dominates, and a simple exponential increase in m is obtained: $\langle S\rangle_m \sim [\beta(1)]^m$. The growth coefficient for $q = 0$ is simply $\beta(q = 0) = 1$. After lengthy but elementary calculations, another leading coefficient for $q = 2$ can be obtained analytically: $\beta(q = 2) = (10+\sqrt{97})/3$.

From the general relationship $\langle S^q\rangle_m \geqslant \langle S\rangle_m^q$ for $q \leqslant 0, q \geqslant 1$, and the monotonic increase of $\langle S^q\rangle_m$ in q, we conclude that $\langle S^q\rangle_m$ increases at least exponentially in m for $q > 0$. In addition, one obtains $\langle S^q\rangle_m \geqslant ((4+\sqrt{13})/3)^{qm}$ for negative q. We therefore postulate that in general the exponential behaviour

$$\langle S^q\rangle_m \sim [\beta(q)]^m \tag{20}$$

holds asymptotically for large m.

In order to evaluate the moments explicitly, numerical calculations based on the iteration procedure in expression (16) have been performed. All numerical results presented in figures 6–8 have been obtained for an initial curvature vector $\boldsymbol{s}_{\mathcal{O}} = (1, 1, 1, 1/(2\sqrt{3}-1))$. In figure 6, the moments of the first 14 generations are presented for five different positive values of q. The numerical results are all well described by the simple exponential variation in (20): all lines shown in figure 6 are straight lines. Whereas for $q = 0, 1, 2$ their slopes correspond to the analytically determined values, for $q = 1/2, 3/2$ the slopes have been estimated numerically. From this excellent quantitative agreement, we conclude that at least for non-negative values of q, the moments converge very fast to their asymptotic exponential increase (20).

Making use of relation (3), the generations m can be uniquely mapped on edge numbers k. The curvature s and area A of a circle are related by $A = \pi/s^2$. Taking into account that for $M\to\infty$ the circle areas coincide with the cell areas, equation (20) can be written as

$$\langle A^{-q/2}\rangle_k \sim k^{\frac{-\ln\beta(q)}{\ln 2}}. \tag{21}$$

For arbitrary values of q, the leading growth coefficients $\beta(q)$ have been estimated numerically from the ratio of the moments in two successive generations, $\langle S^q\rangle_m/\langle S^q\rangle_{m-1}$. In figure 7, the estimated exponents in expression (21) are presented for $q \geqslant -d_{\mathrm{F}}$. The estimates have been

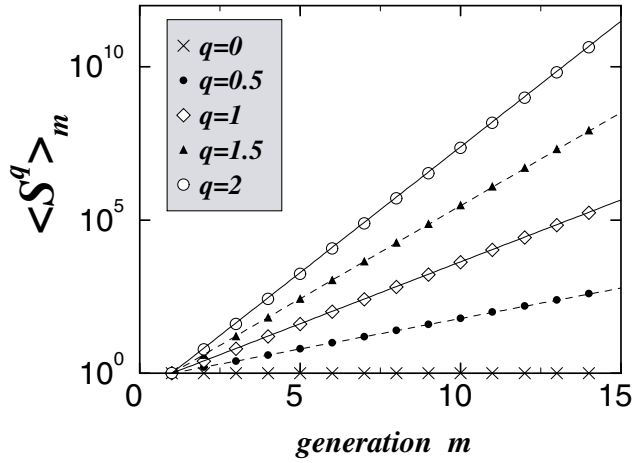

Figure 6. Numerically evaluated moments of the first 14 generations for $q = 0, 0.5, 1, 1.5, 2$. Straight lines are drawn with the analytically determined slopes for $q = 0, 1, 2$. For $q = 1/2, 3/2$, their slope has been determined numerically.

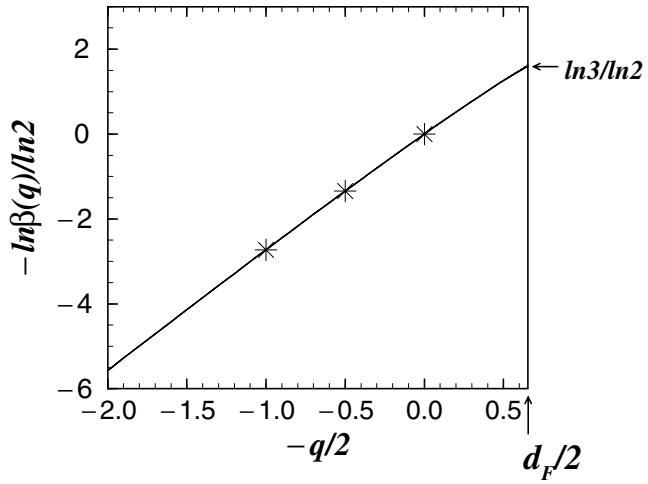

Figure 7. Estimated exponents in equation (21). Stars represent the exact analytical results for $q = 0, 1, 2$.

performed for $m \leqslant 14$. As could be expected from the results presented in figure 6, the ratio shows excellent convergence for positive exponents already for the first generations. With decreasing q, the convergence is slower, but in the representation in figure 7, all errors are still covered by the width of the line.

At first sight, the results presented in figure 7 suggest a linear variation of $\ln \beta(q)$ in q corresponding to a simple scaling (1) of $P(k, A)$. The analytical results for $\beta(q = 0, 1, 2)$, however, clearly disable such a simple scaling since $\beta(2) \neq (\beta(1))^2$. This could be already expected from the fact that the Apollonian packing is not self-similar.

In figure 7, the presentation of the numerically determined leading exponents is restricted to the values $q \geqslant -d_F$, for which the Melzak function introduced after equation (18) diverges. For $q < -d_F$, convergence of this function implies that the total moments $3^{m-1}\langle S^q \rangle_m$ must

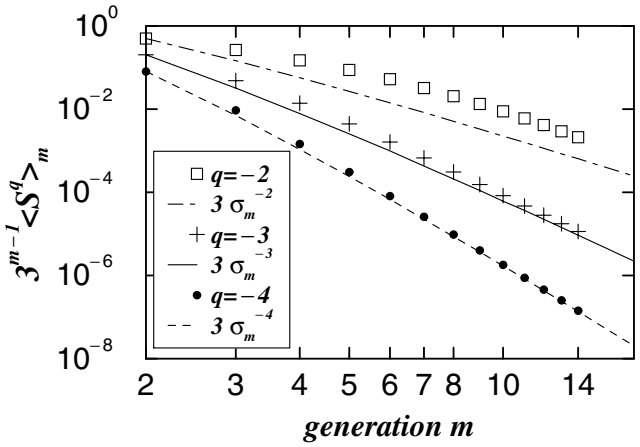

Figure 8. Numerically calculated total moments for $q = -4, -3, -2$.

decay in m, i.e. the leading exponent in (20) cannot be larger than $1/3$:

$$\beta(q < -d_{\mathrm{F}}) \leqslant 1/3. \tag{22}$$

On the other hand, a lower bound of $\langle S^q\rangle_m$ is given by the curvature σ_m of the largest disc in the mth generation:

$$\langle S^q\rangle_m \geqslant 3^{-m}\sigma_m^q. \tag{23}$$

The curvatures σ_m can be determined analytically. Choosing equal curvatures s_{A} of the bounding discs of the packing, the largest discs of each generation always touch two of the bounding discs (see figure 4). From expression (15), a simple recursion relation can be derived: $\sigma_{m+2} - 2\sigma_{m+1} + \sigma_m = 4s_{\mathrm{A}}$. Its solution reads

$$\sigma_m = s_{\mathrm{A}}(1 + 2\sqrt{3}m + 2m^2). \tag{24}$$

Insertion of this result in relation (23) clearly shows that the asymptotic decay of $\langle S^{q<0}\rangle_m$ cannot be faster than $\sim 3^{-m}m^{2q}$. Thus, apart from algebraic corrections the leading exponent has the lower bound

$$\beta(q) \geqslant 1/3. \tag{25}$$

Comparison of relations (22) and (25) yields

$$\beta(q < -d_{\mathrm{F}}) = 1/3.$$

In particular, this result holds for $q = -2$, where the moments measure the average cell area in one generation. Apart from logarithmic corrections, we thus obtain for the average area of a k-sided cell:

$$\langle A\rangle_k \sim k^{\frac{\ln 3}{\ln 2}}. \tag{26}$$

Remarkably, the exponent is identical with the negative exponent of p_k in expression (4). Note that the increase of $\langle A\rangle_k$ is much slower for the Apollonian packing than for the weighted cell areas in the Sierpinski gasket. This can be assigned to the curvature of the bounding triangle and the resulting slow decrease of areas of the largest cells in each generation.

Finally, it should be stressed that expression (26) is valid only in the asymptotic limit of large m. Thus, for its numerical verification and for a quantitative check of the logarithmic corrections, a large number of iterations would be needed. To illustrate this problem, in figure 8

the total moments $3^{m-1}\langle S^q\rangle_m$, $m \leqslant 14$, are shown for three negative values of q. Their lower bounds $3\sigma_m^q$ (24) are added. For $q = -4$, the total moments asymptotically follow their algebraically decaying lower bounds. The quantitative behaviour for $q = -3, -2$, however, appears to be less clear. A quantitative numerical check of their asymptotic behaviour would require extending the calculations to much larger values of m. However, the exponential increase of the number of discs in m clearly disfavours such an extension of the numerical analysis.

5. Conclusions

To conclude, the algebraic increase (2) of the average area of a cell with its number of neighbours appears to be a general property of fractal cellular structures. It suggests a generalization of Lewis's law to the algebraic variation (2) with arbitrary exponents. A similar generalization of Aboav's law describing the topological correlations between neighbouring cells had already been proposed previously [8]. The simple scaling relation (1) proposed in [9] was found to hold only in self-similar Sierpinski cellular structures. In all other cases, multiscaling properties have been obtained. In this paper, we have focused on constructed structures in order to derive rigorous results. Further numerical studies of the metric properties of simulated cellular structures are intended in future. In particular, the random fragmentation model introduced in [4] appears to be a good candidate for a random fractal tessellations.

Acknowledgment

The author is grateful to H Hinrichsen for his interest in this paper, his support and many stimulating discussions.

References

[1] Weaire D and Rivier N 1984 *Contemp. Phys.* **25** 59
Glazier J A and Weaire D 1992 *J. Phys.: Condens. Matter* **4** 1867
Rivier N 1993 Order and disorder in packings and froths *Disorder and Granular Media* ed D Bideau and A Hansen (Amsterdam: Elsevier)
Stavans J 1993 *Rep. Prog. Phys.* **56** 733
[2] Lewis F T 1928 *Anat. Records* **38** 341
Lewis F T 1930 *Anat. Records* **47** 59
Lewis F T 1931 *Anat. Records* **50** 235
[3] Aboav D A 1970 *Metallography* **3** 383
Weaire D 1974 *Metallography* **7** 157
Aboav D A 1980 *Metallography* **13** 43
Lemaître J, Gervois A, Troadec J P, Rivier N, Ammi M, Oger L and Bideau D 1993 *Phil. Mag.* B **67** 347
[4] Delannay R and Le Caër G 1994 *Phys. Rev. Lett.* **73** 1553
[5] Schliecker G and Klapp S 1999 *Europhys. Lett.* **48** 122
[6] Annic C, Troadec J P, Gervois A, Lemaître J, Ammi M and Oger L 1994 *J. Phys. (France) I* **4** 115
[7] Schliecker G 1998 *Phys. Rev.* E **57** R1219
Parfait-Pignol V, Le Caër G and Delannay R 1998 *Eur. Phys. J.* B **4** 499
[8] Le Caër G and Delannay R 1995 *J. Physique* I **5** 1417
[9] Hinrichsen H and Schliecker G 1998 *J. Phys. A: Math. Gen.* **31** L1
[10] Halsey T C, Jensen M H, Kadanoff L P, Procaccia I and Shraiman B I 1986 *Phys. Rev.* A **33** 1141
[11] Okabe A, Boots B and Sugihara K 1992 *Spatial Tessellations* (Chichester: Wiley)
[12] Imai H, Iri M and Murota K 1985 *SIAM J. Comput.* **14** 93
[13] Thomas P B and Deepak D 1994 *J. Phys. A: Math. Gen.* **27** 2257
[14] Soddy F 1936 *Nature* **137** 1021

[15] Coxeter H S M 1961 *Introduction to Geometry* (New York: Wiley)
[16] Söderberg B 1992 *Phys. Rev.* A **46** 1859
[17] Falconer K J 1985 *The Geometry of Fractal Sets* (Cambridge: Cambridge University Press)
[18] Melzak Z A 1969 *Math. Comput.* **23** 169